Chemical Engineering Science 71 (2012) 356–366

Contents lists available at SciVerse ScienceDirect

Chemical Engineering Science

journal homepage: www.elsevier.com/locate/ces

Bio-ethanol steam reforming on Ni based catalyst. Kinetic study

I. Llera, V. Mas, M.L. Bergamini, M. Laborde, N. Amadeo *

Laboratorio de Procesos Catalíticos, Departamento de Ingeniería Química, Facultad de Ingeniería, Pabellón de Industrias, Ciudad Universitaria, 1428 Buenos Aires, Argentina

ARTICLE INFO

Article history:
Received 8 August 2011
Received in revised form
8 December 2011
Accepted 10 December 2011
Available online 27 December 2011

Keywords:
Catalysis
Kinetics
Parameter identification
Steam reforming
Hydrogen
Bioethanol

ABSTRACT

In this work a kinetic study of steam reforming of ethanol using a nickel based catalyst in the temperature range 873–923 K was performed. Conversion monotonically increases with space time and temperature. **At 923 K we obtained more than 5 mol of hydrogen per mole of ethanol**. This hydrogen yield is high compared to values reported in the literature. CO yield increases with the space time and temperature while CO_2 yield has a maximum at 923 K, which coincides with the space time at which the system reaches complete conversion. **At larger residence time CO_2 yield decreases.** CH_4 yield is very low for all conditions studied but a maximum can also be seen with space time. **Both CO_2 and CH_4 are intermediate products, while CO is a final product.** The effect of adding H_2 to the feed was studied. **Analyzing the kinetic results we propose a model involving the following reactions:**

(E1) $CH_3CH_2OH \rightarrow CO + CH_4 + H_2$

(E1) $CH_3CH_2OH + H_2O \rightarrow CO_2 + CH_4 + {}_2H_2$

(R1) $CH_4 + 2H_2O \leftrightarrow CO_2 + 4H_2$

(R2) $CO_2 + H_2 \leftrightarrow CO + H_2O$

The first two involving ethanol are irreversible while the latter two are reversible. **The surface reactions are the rate determining steps**. Kinetic parameters were estimated using commercial software.

1. Introduction

Fuel cell powered vehicles using hydrogen as a fuel are currently being developed in an effort to mitigate the emissions of greenhouse gases such as CO_2, NO_x and hydrocarbons. In addition, hydrogen and the syngas (mixture of hydrogen and carbon dioxides) are both old friends of the chemical industry. Although there exist several routes for hydrogen production from primary fuels, the natural gas steam reforming process is the most used in the chemical industry (J.D. Holladay et al. 2009).

Nevertheless, the clean and non-polluting characteristics of H_2 as a fuel shall depend on the process, the raw material and the source of energy employed for its production.

Among the different raw materials, ethanol presents several advantages in relation to natural availability, storage and handling safety. Its molecule produces 3 molecules of hydrogen, it is a non-toxic liquid at room temperature and it is chemically stable. It can be produced renewably from several biomass sources, including energy plants, waste materials from agro industries or forestry residue materials, organic fraction of municipal solid waste, etc. Besides the bio-ethanol-to-hydrogen system has the significant advantage of being nearly CO_2 neutral, since the produced carbon dioxide is consumed for biomass growth, thus offering a nearly closed carbon loop. In summary, among the various processes and primary fuels that have been proposed in hydrogen production for fuel cell applications, ethanol steam reforming is one of the most attractive (Klouz et al., 2002).

In spite of the apparent simplicity of the stoichiometry reaction for maximum hydrogen production:

$$C_2H_5OH + 3H_2O \rightarrow 6H_2 + 2CO_2$$

ethanol steam reforming for hydrogen production involves a complex reaction system, where several products can be obtained such as ethylene, acetaldehyde (both products are carbon precursors), CO, CO_2, CH_4 and H_2. Therefore the selectivity to hydrogen is affected by many undesirable side reactions.

There are few studies in the literature on kinetic studies of ethanol steam reforming. This is because the system under study is extremely complex (Mas et al., 2008b).

Some kinetic studies have been published in which power law, Eley Rideal like model and Langmuir Hinshelwood model kinetic

* Corresponding author. Tel.: +54 1145763211.
E-mail address: norma@di.fcen.uba.ar (N. Amadeo).

0009-2509/$ - see front matter © 2011 Elsevier Ltd. All rights reserved.
doi:10.1016/j.ces.2011.12.018

expressions are reported (Vaidya and Rodrigues, 2006; Morgensen and Fornango, 2005; Sun et al., 2005; Akande et al., 2006; Sahoo et al., 2007; Akpan et al., 2007; Mas et al., 2008b, 2008c; Graschinsky et al., 2010). Vaidya and Rodrigues (2006) studied the ESR over a Ru/γ–Al_2O_3 catalyst in the temperature range of 873–973 K. Their results showed that the reaction order with respect to ethanol was 1. The rate expression was derived assuming that the decomposition of an activated complex formed during the reaction into intermediate products was the rate determining step (RDS).

Morgensen and Fornango (2005) also studied the ESR at low temperatures (523–573 K) using a copper–nickel catalyst with a Raney-type structure. They suggested that the kinetics fitted a two-step model in which ethanol was dehydrogenated to acetaldehyde in a first-order reaction followed by the decarbonylation of acetaldehyde, which was also first-order.

Sun et al. (2005) studied the ESR at low temperatures (523–623 K) using three nano-sized nickel catalysts: Ni/Y_2O_3, Ni/La_2O_3 and Ni/Al_2O_3. Authors found that the Ni/La_2O_3 catalysts exhibited relatively high activity. They proposed an irreversible first order reaction with respect to ethanol and estimated activation energy values for the three catalysts used.

Akande et al. (2006) performed a kinetic modeling for hydrogen production by catalytic reforming of crude ethanol over a 15%-Ni/Al_2O_3 catalyst. They worked at temperatures in the range of 593–793 K and proposed a kinetic model based on the dissociation of adsorbed crude ethanol as the RDS.

Sahoo et al. (2007) carried out a kinetic study on ESR using Co/Al_2O_3 catalysts. A mechanistic kinetic model using Langmuir–Hinshelwood (L–H) approach was developed considering surface reaction mechanisms for ethanol steam reforming, water gas shift and ethanol decomposition reactions. Authors claim that the formation of acetaldehyde from ethoxy is the RDS for the reforming reaction.

Akpan et al. (2007) proposed mechanistic kinetic models based on Langmuir–Hinshelwood and Eley–Rideal approaches using a Ni-based commercial catalyst. Working with crude ethanol and at temperatures between 673 and 863 K, they used the overall reaction ($C_2H_6O+3H_2O\rightarrow 2CO_2+6H_2$) for the development of kinetic models. It must be noted that authors, using Ni based catalyst and reaction temperatures up to 863 K, do not report the presence of methane and carbon monoxide in the effluent stream.

Mas et al. (2008b) using a Ni (II)–Al(III) lamellar double-hydroxide (LDH) as a catalyst precursor and working at temperatures between 873 and 923 K proposed a power law kinetic expression for the reactions:

$$C_2H_6O+H_2O\rightarrow 2CO+4H_2$$

$$C_2H_6O+3H_2O\rightarrow 2CO_2+6H_2$$

being the reaction orders for ethanol 0.75 and 0.8, respectively, and independent of water concentration for the range of ethanol/water molar ratios used (4.5–5.5).

In another paper (Mas et al., 2008c) the same authors using the Langmuir–Hinshelwood (L–H) approach, proposed a model with four reactions, two of them corresponding to ethanol steam reforming and the other two to methane steam reforming. When high temperatures and/or high water/ethanol feed ratios were used, the system could be reduced to two irreversible ethanol steam reforming reactions. Authors said that there is enough evidence to postulate that both reactives, water and ethanol, are competitively adsorbed on the same type of active site. Nevertheless, these authors claim in both papers that there is no evidence of the occurrence of the WGSR unless in the range of variables studied. On the other hand Graschinsky et al. (2010) performed a kinetic study of ethanol steam reforming reaction on Rh catalysts supported over a spinel structure ($MgAl_2O_4/Al_2O_3$). From the analysis of products distribution the reaction scheme proposed involved the same two irreversible ethanol steam reforming suggested by Mas et al. (2008b) plus WGSR and Methane Steam Reforming. Applying the initial rate method, they demonstrated that in the rate determining step (RDS) two active sites of the same type are involved, in agreement with Mas et al. (2008b).

Although the information published about the mechanism of the ethanol steam reforming reaction is scarce, most authors agree that the first elementary step is the molecular adsorption of ethanol on the active site (Akande et al., 2006; Akpan et al., 2007; Dömök et al., 2007; Mariño et al., 2004; Raskó et al., 2004; Wang et al., 2009). Few others proposed that the ethanol simply decomposes at the active site without molecular adsorption (Busca et al., 2009; Resini et al., 2009; Diagne et al., 2002; Sahoo et al., 2007).

Basic catalysts promote the dehydrogenation to acetaldehyde and acid catalysts favor the dehydration to ethylene (Martin and Duprez, 1997). Fatsikostas and Verykios (2004) demonstrated that γ-Al_2O_3 was very selective for ethylene. Modifying the alumina with Mg, it acquires basic features that allow greater mobility of OH groups favoring ethanol steam reforming reaction (Aupretre et al., 2002). Comparing with catalysts supported on alumina, those catalysts supported on spinel exhibit a slightly higher basicity, whereas the surface acidity is strongly reduced. In summary, the acidic and basic properties of supports are essential parameters that directly affect the primary selectivity to acetaldehyde or ethylene. Ethylene would be produced only on the support, with an essential role of the acidic sites in olefin formation. The dehydrogenation, on the other hand, mainly occurs over metallic sites (Aupretre et al., 2005). Moreover, the ethylene produced over the catalyst is rapidly decomposed to hydrocarbon fragments (coke) while the acetaldehyde is further transformed into reaction products (Sahoo et al., 2007).

Water activation can follow different routes. Many authors propose the dissociative adsorption to OH and H (Mariño et al., 2004; Raskó et al., 2004; Sahoo et al., 2007). Other authors have proposed that water in the gas phase reacts with adsorbed species following an Eley–Rideal mechanism (Akande et al., 2006; Dömök et al., 2007). Nevertheless this kind of mechanism has a very poor probability of occurrence (Vanicce, 2005). The spinel support promotes the water activation and possesses very mobile OH groups favoring the reaction with the CHxOy species adsorbed on the metal particles (Aupretre et al., 2005).

Based on the results obtained by Mas et al. (2008b, 2008c) and using a range of operating variables broader than that employed by these authors, the aim of this work is to go deeper into the kinetic study of ethanol steam reforming, postulate a kinetic scheme and determine the kinetic parameters of the reactions involved and, if possible elucidate the occurrence of the WGSR.

2. Experimental

2.1. Catalyst

A Ni(II)–Al(III) lamellar double hydroxide (LDH) was used as catalyst precursor. This precursor was synthesized by the urea method aging mixed aluminum(III)–nickel(II)–urea solutions at 363 K in screw-capped plastic bottles, which were placed in a thermostatized water bath preheated at working temperature for 24 h. The Ni(II)/Al(III) molar ratio in the solution was 2.33, value typical of takovite. Details of the preparation method are given elsewhere (Mas et al., 2008a, 2008b). Catalyst was characterized by chemical analysis, sorptometry, TGA and XRD measurements.

The reduced NiAl sample had a specific area of 100 m^2/g and the mean size of the Ni metallic crystallites was estimated using Scherrer's equation, being close to 5 ± 1 nm. The complete experimental procedure and catalyst characteristics are described in detail in Mas et al. (2008a).

2.2. Catalytic runs

The catalytic evaluation was performed in a quartz reactor of 4 mm i.d., located in an electric oven. Reaction temperature was measured by a thermocouple placed inside the catalytic bed. The reactants, a mixture of water and ethanol, were fed in liquid state by a syringe HPLC type pump. The mixture was evaporated in an electric oven at 623 K and diluted afterwards with an argon-carrier stream (350 ml min^{-1}). The catalyst was ground to a diameter between 44 and 88 μm with the aim of avoiding any diffusion limitation inside the particle and diluted with inert material of the same diameter to avoid any temperature gradient within the catalytic bed. Prior to the catalytic evaluation, experiments were carried out in order to verify the negligible contribution of homogeneous phase reaction and the absence of external and internal diffusion limitations (Mas et al., 2008b). The plug flow condition was achieved by providing $L/Dp \geq 50$ and $D/Dp \geq 30$ (Froment and Bishoff, 1990). The activation of the precursor was carried out by reduction with pure hydrogen during 2 h with a ramp of 10 K min^{-1} to reach the activation temperature of 923 K.

All the experiments were performed at atmospheric pressure.

The analysis of the feed and the products stream were carried out online by gas chromatography in an Agilent Chromatograph, Model GC 6820 with two columns (Innowax and Carbonplot) and FID and TCD detectors.

The steady state condition was reached approximately after an hour of reaction. The reproducibility of experimental results was checked and the experimental error was less than 2%. Carbon balance was close to 95% in all experiments, which corroborates the following two observations: no carbon formation was detected and good stability of the catalyst during a run time (8 h).

The catalytic results are discussed in terms of

$$\text{Ethanol conversion}: \ \chi = \left(1 - \frac{y_{ET}^{out}}{y_{ET}^{in}}\right)100 \tag{1}$$

$$\text{Water conversion}: \ \chi_{H_2O} = \left(1 - \frac{y_{H_2O}^{out}}{y_{H_2O}^{in}}\right)100 \tag{2}$$

$$\text{Selectivity}: \ S_j = \left(\frac{y_j^{out} - y_j^{in}}{(y_{Et}^{in} - y_{Et}^{out})a_j}\right)100 \tag{3}$$

$$\text{Yield}: \ R_j = \left(\frac{y_j^{out} - y_j^{in}}{y_{Et}^{in} a_j}\right)100 \tag{4}$$

$$\text{Space time}: \ \theta_V = \frac{w}{F_{V,T}} \tag{5}$$

Experimental conditions used in this work are shown in Table 1.

3. Results and discussion

In a previous paper we studied this reaction with the same catalyst in a narrower range of space time in which the ethanol conversion was less than one (Mas et al., 2008b, 2008c). In this work we employed larger spaces times. Ethanol and water conversion vs. space time, at different temperatures, are shown in Fig. 1. As it can be seen ethanol conversion increases with temperature and space time. Particularly at the highest temperature the total ethanol conversion is reached at a space time of 0.015 min mg/ml. Water conversion also increases with temperature and space time for space times lower than 0.015 min mg/ml. At 923 K and space times greater than 0.015 the water conversion remains constant in correspondence with the total conversion of ethanol or decreases slightly due to the water formation through the reverse WGS reaction favored at the higher temperature.

Table 1
Experimental conditions.

Variable	Units	Operative conditions
T	[K]	873–923
P	[atma]	1
w	[mg]	2.0–11.0
$F_{V,dry}$	[ml/min]	350
θ_V	[min mg/ml]	0.0050–0.0276
$y_{H_2O}^{in}$	–	0.090
y_{et}^{in}	–	0.016
H_2O:ethanol (mol/mol)	–	5.5:1
Particle size	[μm]	44–88
Inert/catalyst	–	10:1

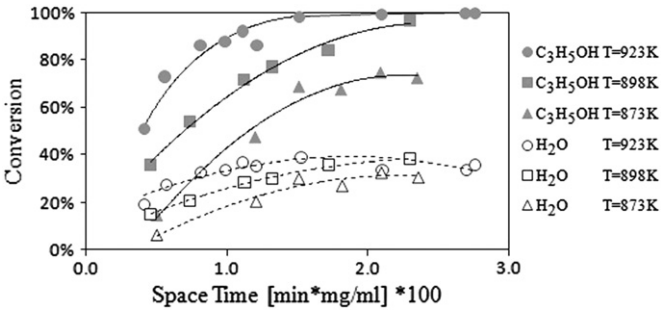

Fig. 1. Ethanol and water conversion vs. space time at different temperatures.

Previous work using Ni as catalyst (Comas et al., 2004; Mas et al., 2008a, 2008b, 2008c; Vizcaino et al., 2008), let us elucidate a system of reactions involving ethanol, ethylene and acetaldehyde as intermediates and CO, CO_2 and CH_4 as products of ethylene and acetaldehyde steam reforming. This system can be simplified if one considers that the amounts of ethylene and acetaldehyde in the experiments are negligible (less than 1% in all experiments):

E1: $C_2H_5OH \rightarrow CO + CH_4 + H_2$

E2: $C_2H_5OH + H_2O \rightarrow CO_2 + CH_4 + 2H_2$

CO and CO_2 yields vs. space time at different temperatures are shown in Fig. 2. CO_2 yield follows a similar pattern to the hydrogen yield at 873 K and 898 K. At 923 K it is observed that CO_2 yield reaches a maximum. This maximum occurs when ethanol is completely converted (see Fig. 1). In what follows we call this experimental condition as Condition *. CO yield follows a pattern similar to CO_2 when the conversion is not complete, i.e., increases monotonically. When the conversion is complete, at 923 K and space times greater than 0.015 min mg/ml, CO yield continues to increase, as opposed to what happens with CO_2. Once the ethanol is completely consumed the system tends to a net consumption of CO_2 and conversely, CO production is increased. It can be said that CO_2 is an intermediate product and CO is an end product. This behavior would be interpreted by the inverse of the WGS reaction:

$CO_2 + H_2 \leftrightarrow CO + H_2O$

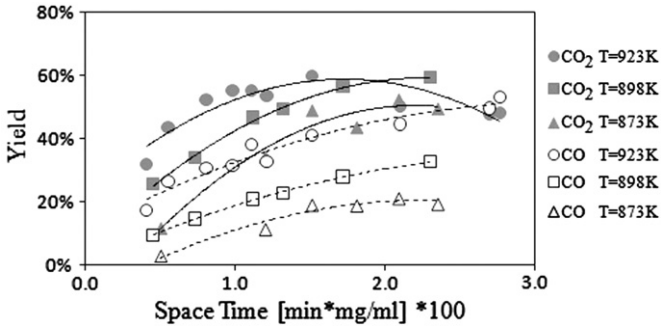

Fig. 2. CO and CO_2 yields vs. space time at different temperatures.

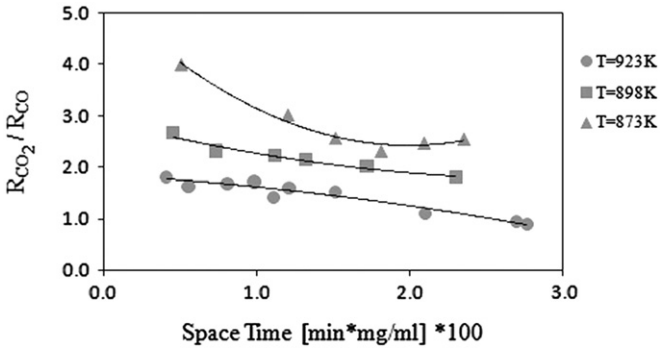

Fig. 3. CO_2/CO molar ratio vs. space time for different temperatures.

Mas et al. (2008b) did not observe this behavior because the maximum space time used in that work was that corresponding to complete conversion (0.015 min mg/ml). As no maximum in CO_2 or CO was observed, Mas et al. (2008b) concluded that WGSR did not occur.

CO_2/CO molar ratio vs. space time for different temperatures is shown in Fig. 3. It is clear that the system has a CO_2/CO molar ratio higher than 1 in all the temperature range studied, this ratio being higher at lower temperatures. For all temperatures studied, this ratio decreases when space time increases. Both behaviors are in agreement with the thermodynamics of the inverse water gas shift reaction (WGS).

Hydrogen yield vs. space time at different temperatures are shown in Fig. 4. Hydrogen yield increases with temperature and space time. At 923 K and space times larger than 0.015 min mg/ml, hydrogen yield remains constant in agreement with the complete conversion of ethanol and then decreases slightly due to the existence of the inverse WGSR. The maximum hydrogen yield obtained is higher than 80%, equivalent to 5.1 mol of H_2 per mol of ethanol. This hydrogen yield is high compared to those obtained by other authors. Profeti et al. (2009), working with CeO_2–Al_2O_3 catalysts modified with noble metals such as Pt, Ir, Pd and Ru, report an hydrogen yield of 60% at 600 °C; Batista et al. (2004) using Co/Al_2O_3 and Co/SiO_2 catalysts also obtained yields of 60%. Sun et al. (2005) employing Ni/Y_2O_3, Ni/La_2O_3 and Ni/Al_2O_3 catalysts and working at 280–320 °C report hydrogen yields in the range of 43–54%.

Methane yield at 923 K is also shown in Fig. 4. It can be seen that it is very low in the range of space time analyzed. It presents a maximum, which occurs when ethanol still exists in the system, indicating that methane is an intermediate compound.

Selectivity of all the compounds vs. temperature for two space times are shown in Fig. 5. H_2 selectivity is almost constant when varying the space time and decreases slightly with temperature.

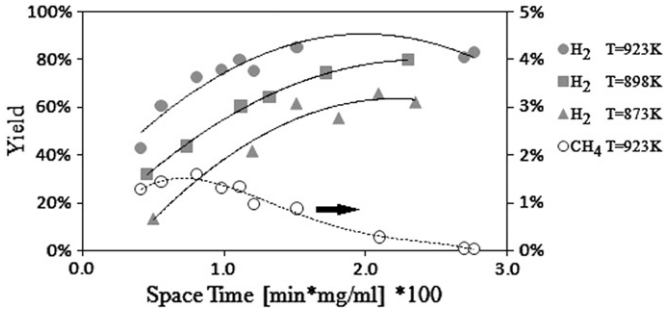

Fig. 4. Hydrogen and methane yields vs. space time at different temperatures.

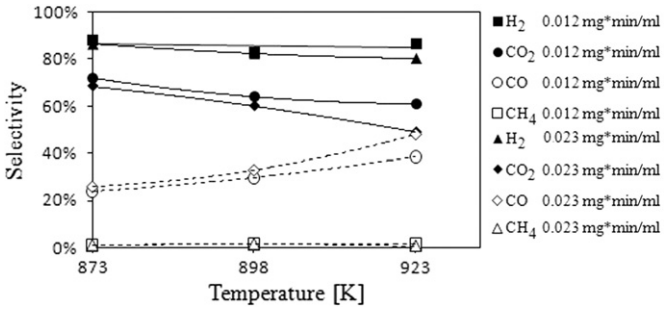

Fig. 5. Selectivity of all the compounds vs. temperature for two space times.

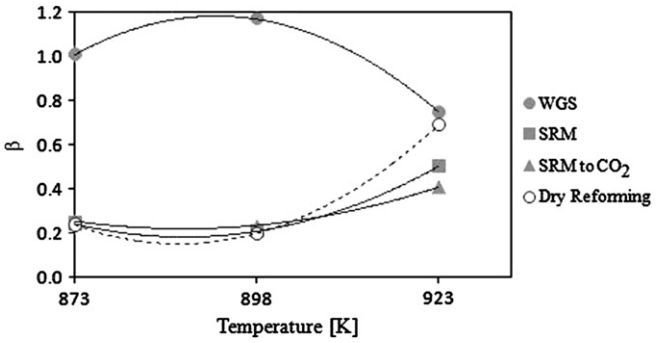

Fig. 6. β_i vs. temperature at the highest space time.

CO_2 selectivity decreases with increasing temperature. On the contrary, CO selectivity increases with temperature. This, as explained above, is consistent with the thermodynamics of the inverse WGS reaction, which predicts that the distribution of products favors the presence of CO over CO_2 at higher temperatures.

If only reactions E1 and E2 were considered it should be verified that $SCH_4 = SCO + SCO_2$. However it can be seen that $SCH_4 < SCO + SCO_2$ and on the other hand the analysis in Fig. 4 indicates that methane is an intermediary compound. It is therefore necessary to consider reactions involving the consumption of methane. If the formation of coal is discarded, the steam reforming reactions (MSR) and the dry reforming could be considered (MDR):

MSR_{CO} $CH_4 + H_2O \leftrightarrow CO + 3H_2$

MSR_{CO2} $CH_4 + 2H_2O \leftrightarrow CO_2 + 4H_2$

MDR $CH_4 + CO_2 \leftrightarrow 2CO + 2H_2$

It can be noted that E1 and E2 reactions are assumed as irreversible while WGSR, MSR_{CO}, MSR_{CO2} and MDR reactions are

Table 2
Experimental conditions for the experiments using hydrogen in the feed (the parameters that kept the same values as those shown in Table 1 are not shown in this table).

Variable	Units	Operative conditions
w	[mg]	4.7
$F_{V,dry}$	[ml/min]	500
θ_V	[min mg/ml]	0.0086
$y^{in}_{H_2O}$	–	0.060
y^{in}_{et}	–	0.0109

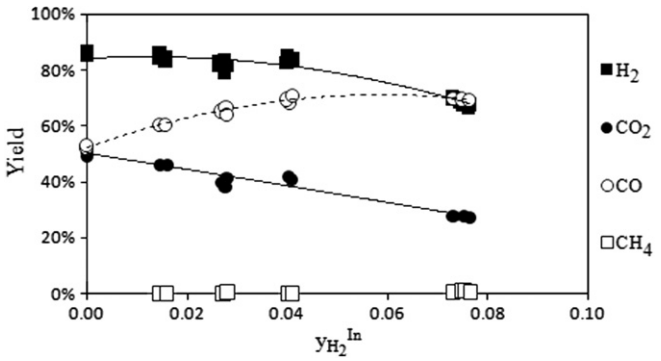

Fig. 7. Product distribution vs. hydrogen molar fraction in the feed at two temperatures.

assumed as reversible. Let us define $\beta_i = Q_i/K_i^{eq}$ where $Q_i = \pi y_j^{\gamma ij}$. In Fig. 6, β_i vs. temperature at the high space time used is shown. It can be concluded that the four reversible reactions are far from the equilibrium. In addition it can be seen that WGS reaction or its inverse may occur depending on the values of space time and temperature.

The effect of adding hydrogen to the feed on the products distribution was analyzed. The operative conditions for this series of experiments are shown in Table 2.

The product distribution vs. hydrogen molar fraction in the feed is shown in Fig. 7 for one temperature. It is observed that H_2 yield decreases with increasing hydrogen molar fraction. CO_2 yield decreases and CO yield increases slightly when increasing the molar fraction of H_2 in the feed. It can also be seen that there is a higher proportion of CO/CO_2 when the amount of hydrogen in the feed increases. CH_4 yield is negligible compared to other species. These trends appear to be in agreement with the inverse WGSR.

3.1. Kinetic model

The following hypotheses are assumed to narrow the wide variety of possible models.

1. All species are adsorbed on the same type of active site. As demonstrated in previous works for the same catalyst (Mas et al., 2008b) and for a rhodium based catalyst (Graschinsky et al., 2010) and similar operative conditions, ethanol, water and methane are adsorbed and react on the same type of active site. It means that at least two active sites must be involved in the controlling step.
2. The existence of a controlling elementary step in the reaction is assumed. This allows solving the system using the RDS method (Rate Determining Step).
3. The experiments were conducted under conditions such that there was no appreciable coke formation and in the transient larger amounts of acetaldehyde to ethylene were observed, so that the formation of ethylene and the reactions involving the formation and/or consumption of coke are discarded.
4. The ethanol decomposition only proceeds through the formation of acetaldehyde and its decomposition on the catalyst surface. At steady state the amounts of acetaldehyde are negligible ($<1\%$) therefore the model is simplified by assuming that the desorption of acetaldehyde does not occur.
5. The number of reactions is limited to a minimum. In this way a system as simple as possible is achieved, with fewer parameters, more reliable and robust to estimate them. When ethanol is almost entirely exhausted the system is composed of five species: H_2O, CH_4, CO, CO_2 and H_2. In turn, these five species arise from the proper combination of three different atomic species C, O and H. Therefore, two linearly independent reactions to describe the equilibrium, which the system tends are needed. However, kinetically the system is sensitive to the presence of more reactions. In conclusion at least two reversible reactions should be considered. As proposed earlier, WGS is one of these reversible reactions, while the remaining will come from the MSR_{CO}, MSR_{CO2} and MDR reactions. Of these three reactions the steam reforming reaction to produce CO_2 (MSR_{CO2}) is chosen. The justification for this choice is explained in Appendix A. Under these assumptions the kinetic model consists of the following four reactions:

$$E1: C_2H5OH \rightarrow CO + CH_4 + H_2$$

$$E2: C_2H_5OH + H_2O \rightarrow CO_2 + CH_4 + 2H_2$$

$$R1: CH_4 + 2H_2O \leftrightarrow CO_2 + 4H_2$$

$$R2: CO_2 + H_2 \leftrightarrow CO + H_2O$$

The literature reports that the possible controlling steps I are C–C rupture (Akande et al., 2006) and surface reactions (Mas et al., 2008b; Sahoo et al., 2007; Graschinsky et al., 2010). If the break of the C–C bond is the controlling step, the methane steam reforming and WGSR would be in equilibrium. However, as concluded before, both reactions are far from equilibrium. Then surface reactions are proposed as RDS. Defining $\Leftrightarrow$ as reversible step in quasi-equilibrium, $\leftrightarrow$ as reversible stage and $\rightarrow$ as an irreversible stage, the model, based on published information, which it was detailed in the introduction, is defined as

$$\begin{aligned}
&(01)\quad C_2H_5OH + (a) &&\Leftrightarrow && C_2H_5OH(a)\\
&(02)\quad C_2H_5OH(a) + (a) &&\Leftrightarrow && C_2H_5O(a) + H(a)\\
&(03)\quad C_2H_5O(a) + (a) &&\Leftrightarrow && C_2H_4O(a) + H(a)\\
&(04)\quad C_2H_4O(a) + (a) &&\Leftrightarrow && CH_3(a) + CHO(a)\\
&(05)\quad CH_3(a) + (a) &&\Leftrightarrow && CH_2(a) + H(a)\\
&(06)\quad CH_2(a) + (a) &&\Leftrightarrow && CH(a) + H(a)\\
&(07)\quad CHO(a) + (a) &&\rightarrow && CO(a) + H(a)\\
&(08)\quad CH_3(a) + H(a) &&\Leftrightarrow && CH_4(a)\\
&(09)\quad CHO(a) + OH(a) &&\rightarrow && CO_2(a) + H_2(a)\\
&(10)\quad CH(a) + 2OH(a) &&\leftrightarrow && CO_2(a) + H_2(a) + H(a)\\
&(11)\quad CO_2(a) + H(a) &&\leftrightarrow && CO(a) + OH(a)\\
&(12)\quad H_2O + (a) &&\Leftrightarrow && H_2O(a)\\
&(13)\quad H_2O(a) + (a) &&\Leftrightarrow && H(a) + OH(a)\\
&(14)\quad CH_4(a) &&\Leftrightarrow && CH_4 + (a)\\
&(15)\quad CO(a) &&\Leftrightarrow && CO + (a)\\
&(16)\quad 2H(a) &&\Leftrightarrow && H_2(a) + (a)\\
&(17)\quad CO_2(a) &&\Leftrightarrow && CO_2 + (a)\\
&(18)\quad H_2(a) &&\Leftrightarrow && H_2 + (a)
\end{aligned}$$

Solving the system we obtain

$$r_{E1} = \frac{k_{E1} y_E y_{CH_4}^{-1} y_{H_2}^{-(1/2)}}{DEN^2}$$

$$r_{E2} = \frac{k_{E2} y_E y_{H_2O} y_{CH_4}^{-1} y_{H_2}^{-1}}{DEN^2}$$

$$r_{R1} = \frac{k_{R1} y_{H_2O}^2 y_{CH_4} y_{H_2}^{-(5/2)} (1-\beta_{R1})}{DEN^3}$$

$$r_{R2} = \frac{k_{R2} y_{CO_2} y_{H_2}^{1/2} (1-\beta_{R2})}{DEN^2}$$

$$\begin{aligned} DEN = 1 &+ K_{Et} y_{Et} + K_{Etx} y_{Et} y_{H_2}^{-(1/2)} + K_{Ac} y_{Et} y_{H_2}^{-1} + K_{CHO} y_{Et} y_{CH_4}^{-1} y_{H_2}^{-(1/2)} \\ &+ K_{CH_3} y_{CH_4} y_{H_2}^{-(1/2)} + \cdots + K_{CH_2} y_{CH_4} y_{H_2}^{-1} + K_{CH} y_{CH_4} y_{H_2}^{-(3/2)} \\ &+ K_{H_2O} y_{H_2O} + K_{OH} y_{H_2O} y_{H_2}^{-(1/2)} + K_{CH_4} y_{CH_4} + \cdots \\ &+ K_{CO} y_{CO} + K_{CO_2} y_{CO_2} + K_H y_{H_2}^{1/2} + K_{H_2} y_{H_2} \end{aligned}$$

The meaning of the kinetics coefficients and the equilibrium constants is given in Appendix B.

This model has 36 parameters, in which the molar fraction of methane and hydrogen cannot be null. It is assumed that $y_{CH_4}^{inlet} = 0.0001$ and $y_{H_2}^{inlet} = 0.0005$. These values were determined in homogeneous phase, while loading the reactor with inert only.

3.2. Parameter estimation

Mass balance of the j compound in a plug flow reactor in steady state is given by

$$\frac{dF_j}{dw} = \sum_i \alpha_{ij} r_i$$

$$F_j = F_j^{in} + \sum_i \alpha_{ij} X_i \Rightarrow F_T = F_T^{in} + \sum_i \overline{\alpha}_i X_i$$

where

$$\overline{\alpha}_i = \sum_{j=1}^{s} \alpha_{ij}$$

If the system is diluted, as in our case, we can raise the mass balance in terms of molar fractions

$$\frac{dy_j}{d\vartheta} = \sum \alpha_{ij} r_i$$

where $\vartheta = w/F_T^{inlet}$, $y_j = F_j/F_T^{inlet}$ and r_i is the reaction rate of the i reaction.

Once the kinetic model is determined we have a set of nonlinear differential equations (mass balances for each species), which indicate the variation of each species along the reactor as a function of temperature, the kinetic parameters of the model and the mole fractions of all species. The system to solve consists of 6 species (S=6): CH_3CH_2OH, H_2O, CH_4, CO, CO_2 and H_2 and 220 experiments (N=220), i.e. 1320 observed experimental data. To estimate the parameters a commercial software Athena Visual Studio 12.0c and a Matlab-based software were used. A brief description of the methodology employed to solve the system of differential equations is presented in Appendix C.

By analyzing together the results obtained for the three temperatures it must be verified that the activation energies of elementary steps are positive and, on the other hand it must be true that

- Adsorption is always an exothermic process, then $\Delta H_{ads}^0 < 0$;
- Upon adsorption the entropy must decrease, even in a dissociative adsorption, then $\Delta S_{ads}^0 = S_{ads}^0 - S_g^0 < 0$;
- An atom or molecule cannot lose more entropy than it originally possessed in the gas phase, i.e. $|\Delta S_{ads}^0| < S_g^0$, it means that the entropy of the adsorbed body must be positive.

In Table 3 values of the kinetic parameters obtained are shown. The values of activation energy and reaction enthalpy for the different elementary steps are given in Table 4. It can be seen that the estimated values respond satisfactorily to exothermic adsorptions and endothermic desorptions and all activation energies are positive.

The goodness of fit obtained with this model is 0.95218. The estimated values for this model are in the order of those reported by other authors, as shown in Tables 5–7. This could be a criterion, besides the goodness of fit, which strengthens the model. The differences between the values found in different works can be attributed, in some cases, to the different catalysts used, in others to differences in the proposed reaction mechanism (Mas et al., 2008c). Finally, in cases where the activation energy takes much smaller values, presumably experimental conditions were not suitable for the determination of kinetic parameters, i.e. conditions of chemical control.

Molar fractions determined with the model vs. experimental molar fractions for each species are shown in Figs. 8 and 9 (charts

Table 3
Values of the kinetics parameters.

$k_{i(T)} = k_{i(898.15K)} e^{-(Ea_i/R)((1/T)-(1/898.15K))}$[=](mol/min mg) $K_{i(T)} = K_{i(898.15K)} e^{-(\Delta H_i/R)((1/T)-(1/898.15K))}$[=](a dimensional)		Ea_i, ΔH_i[=](kJ/mol)	
$k_{E1(898.15K)}$	1.13E−07	Ea_{E1}	122.9
$k_{E2(898.15K)}$	3.06E−07	Ea_{E2}	195.5
$k_{R1(898.15K)}$	2.48E−03	Ea_{R1}	174.0
$k_{R2(898.15K)}$	9.12E−04	Ea_{R2}	166.3
$K_{Et(898.15K)}$	8.76E−27	ΔH_{Et}	−601.4
$K_{Etx(898.15K)}$	1.93E−22	ΔH_{Etx}	−207.9
$K_{CHO(898.15K)}$	2.10E−01	ΔH_{CHO}	−410.4
$K_{Ac(898.15K)}$	8.76E−27	ΔH_{Ac}	−83.1
$K_{CH_2(898.15K)}$	1.93E−22	ΔH_{CH_2}	−118.4
$K_{CH(898.15K)}$	3.05E−01	ΔH_{CH}	−360.7
$K_{CH_3(898.15K)}$	1.93E−22	ΔH_{CH_3}	−126.8
$K_{H_2O(898.15K)}$	1.93E−22	ΔH_{H_2O}	−83.1
$K_{OH(898.15K)}$	1.93E−22	ΔH_{OH}	−145.5
$K_{CH_4(898.15K)}$	6.34E−18	ΔH_{CH4}	−86.1
$K_{CO(898.15K)}$	1.93E−22	ΔH_{CO}	−83.1
$K_{H(898.15K)}$	8.76E−27	ΔH_H	−247.4
$K_{CO_2(898.15K)}$	1.93E−22	ΔH_{CO_2}	−83.4
$K_{H_2(898.15K)}$	1.93E−22	ΔH_{H_2}	−931.2

of parity). It can be seen that the estimation of the water molar fraction is within ±10%, while for hydrogen the fit is satisfactory for the largest proportion of events.

For C_2H_5OH, CH_4, CO and CO_2, where the molar fractions are lower than those of water and hydrogen, the fit has larger deviations, with a tendency to model a larger proportion of ethanol and CO_2 and a lower tendency of CO relative to those observed experimentally.

Finally, the fixed bed reactor used in the experiments was simulated assuming plug flow model and using the kinetics expressions and the kinetics parameters obtained in this work. The experimental and the estimated values at 923 K are shown in Fig. 10. It can be appreciated that the fit is quite satisfactory.

Table 4
Activation energy and enthalpy of elementary steps.

ΔH_1^{ads}	−601.38	E_{11}	497.07
ΔH_2	146.09	E_{-11}	799.41
ΔH_3	−34.86	ΔH_{12}^{ads}	−83.10
ΔH_4	−338.22	ΔH_{13}	−309.79
ΔH_5	−238.99	ΔH_{14}^{des}	86.10
ΔH_6	−121.26	ΔH_{15}^{des}	83.10
E_7	329.69	ΔH_{16}	−436.36
ΔH_8	288.09	ΔH_{17}^{des}	83.39
E_9	835.86	ΔH_{18}^{des}	931.14
E_{10}	1435.92	en [kJ/mol]	
E_{-10}	2594.37		

Table 5
Activation energy values reported in the literature for SRM to CO_2 (R1).

Reference	*T* [K]	Catalyst	Kinetics	Activation energy [kJ/mol]
This work	873–923	Ni–Al–O	LHHW	174.0
Hou and Hughes (2001)	598–823	$Ni_{16\%}/\alpha$-Al_2O_3	LHHW	109.4
Mas et al. (2008c)	873–923	Ni–Al–O	LHHW	213.9
Bousiffi and Gunn (2007)	873–1113	Ni/Al_2O_3	Power law	12.2
Xu and Froment (1989)			LHHW	243

4. Conclusions

In this work ethanol steam reforming kinetics using a Ni based catalyst was studied in the temperature range 873–923 K.

The catalyst proved to be active towards the ethanol steam reforming being able to achieve conversions of 100% ethanol. Conversion monotonically increases with space time and temperature.

At 923 K we obtained more than 5 mol of hydrogen per mole of ethanol. This hydrogen yield is high compared to values reported in the literature.

It was observed that CO yield increases with the space time and temperature while CO_2 yield has a maximum at 923 K, which coincides with the space time at which the system reaches complete conversion. At larger residence times CO_2 yield

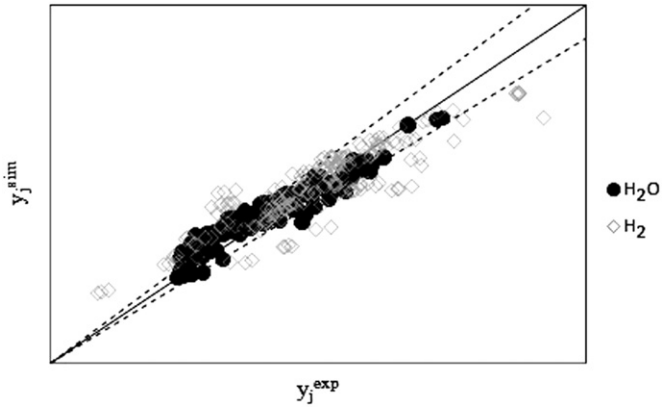

Fig. 8. Chart of parity for H_2O and H_2.

Table 6
Activation energy values reported in the literature for WGSR.

Reference	*T* [K]	Catalyst	Kinetics	Activation energy [kJ/mol]
This work	873–923	Ni–Al–O	LHHW	166.3
Hou and Hughes (2001)	598–823	$Ni_{16\%}/\alpha$-Al_2O_3	LHHW	88
Phatak et al. (2007)	453–618	$Pt_{1\%}/Al_2O_3$	Power law	104
Phatak et al. (2007)	453–618	$Pt_{1\%}/CeO_2$	Power law	111
Graschinsky et al. (2010)	773–873	$Rh(1\%)MgAl_2O_4/Al_2O_3$	LHHW	107
Sahoo et al. (2007)	673–973	Co/Al_2O_3	LHHW	71.3

Table 7
Activation energy values reported in the literature for E1 and E2 reactions.

Reference	T [K]	Catalyst	Kinetics	Activation energy [kJ/mol]	
				*E*1	*E*2
This work	873–923	Ni–Al–O	LHHW	122.9	195.5
Mas et al. (2008c)	873–923	Ni–Al–O	LHHW	278.7	235
Sahoo et al. (2007)	673–973	$Co_{15\%}/Al_2O$	LHHW	71.3	–
Morgensen and Fornango (2005)	523–573	Cu/Ni	Power law	–	149
Graschinsky et al. (2010)	773–873	$Rh(1\%)MgAl_2O_4/Al_2O_3$	LHHW	85.9	418
Vaidya and Rodrigues (2006)*	873–973	Ru/γ-Al_2O_3	Power law	96	
Akande et al. (2006)*	593–793	Ni/Al_2O_3	ER	4.41	
Akpan et al. (2007)*	673–863	Ni-based commercial catalyst	LH-ER	59.7	
Sahoo et al. (2007)**	673–973	Co/Al_2O_3	LHHW	82.7	

* These works considered the overall reaction: $C_2H_6O+3H_2O=2CO_2+6H_2$.
** This work considered the overall reaction, water gas shift and ethanol decomposition.

decreases. On the other hand, CH_4 yield is very low for all conditions but a maximum can also be seen with space time. From these observations it can be concluded that both CO_2 and CH_4 are intermediate products, while CO is a final product.

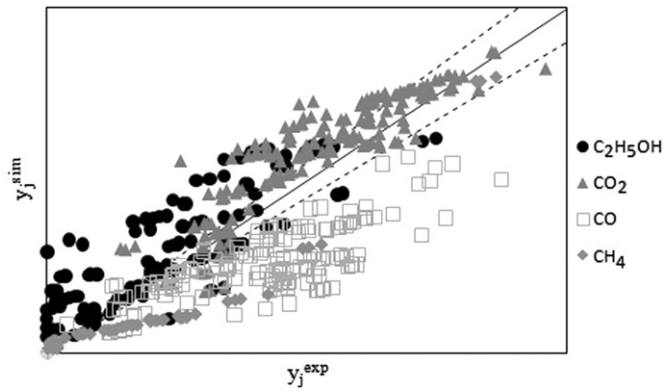

Fig. 9. Chart of parity for C_2H_5OH, CH_4, CO and CO_2.

The CO_2 selectivity increases while CO selectivity decreases with increasing temperature. This is consistent with the thermodynamics of the WGS, which predicts that the higher the temperature, the more the presence of CO over CO_2 is favored. **WGSR or its inverse may occur depending on the value of space time and temperature.**

When H_2 is added to feeding, the H_2 and CO_2 yields decrease and CO yield increases.

A LHHW kinetic model assuming a series of elementary steps was developed. RDS (Rate Determining Step) method was used being an effective and simple technique to apply systematically. The reactions involved in this model are as follows:

(E1) $CH_3CH_2OH \rightarrow CO+CH_4+H_2$

(E2) $CH_3CH_2OH+H_2O \rightarrow CO_2+CH_4+2H_2$

(R1) $CH_4+2H_2O \leftrightarrow CO_2+4H_2$

(R2) $CO_2+H_2 \leftrightarrow CO+H_2O$

Based on experimental evidence it was assumed that in each of the four reactions, surface reaction was the determining step (RDS). All model parameters take allowable values and the goodness of fit for the 1320 experimental data is 0.95218.

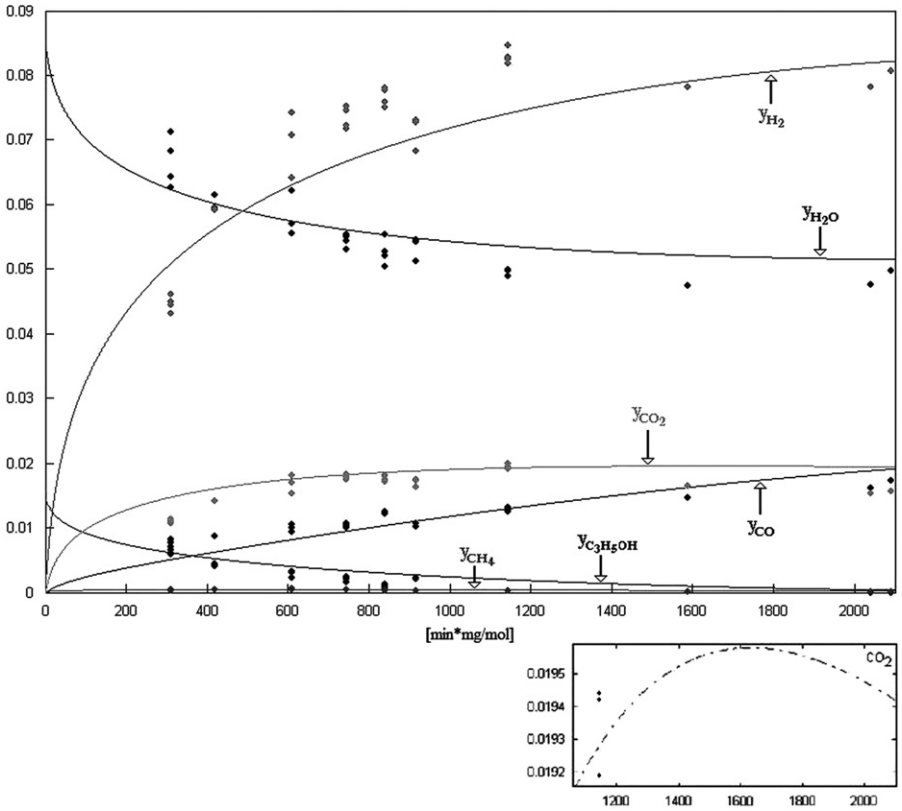

Fig. 10. Experimental data and estimated data vs. space time. T: 923 K; $y_{et}^{in}=0.016$; $y_{H_2O}^{in}=0.088$.

Table A.1
Values of β for WGS, SRM, in the condition*.

β^*			
WGS	**MSR_{CO}**	**MSR_{CO2}**	**MDR**
$CO+H_2O \leftrightarrow CO_2+H_2$	$CH_4+H_2O \leftrightarrow CO+3H_2$	$CH_4+2H_2O \leftrightarrow CO_2+4H_2$	$CH_4+CO_2 \leftrightarrow 2CO+2H_2$
1.32	0.1	0.25	0.14

Matlab simulations showed that the model is able to adjust the trends of variation of the molar fractions observed experimentally.

Appendix A

Throughout the temperature range studied the yields of CO and CO_2 are monotonically increasing while the ethanol conversion is not complete. Instead there is a maximum yield of CO_2 when the ethanol conversion is complete. In this case the system conditions correspond to the so-called Condition *, which must be fulfilled:

$$\left.\frac{dy_{CO_2}}{d\theta}\right|_* = \sum_i \alpha_{i,CO_2} r_i^* = 0 \quad \wedge \quad \left.\frac{d^2 y_{CO_2}}{d\theta^2}\right|_* < 0 \tag{A.1}$$

Experimentally it was observed that $y^*_{Et} \to 0$, then irreversible reactions involving the ethanol also tend to zero. On the other hand the hypothesis 5 (see text) postulated the existence of only two reversible reactions. Then Eq. (A.1) becomes

$$\left.\frac{dy_{CO_2}}{d\theta}\right|_* = \alpha_{R1,CO_2} r^*_{R1} + r^*_{WGS} = 0 \tag{A.2}$$

where R1 is any reversible reaction containing methane as a reactant: MSRCO, MSR_{CO2} and MDR. Values of β for these reactions and for WGSR in the condition * are given in Table A.1. It can be seen that $\beta^*_{WGS} \neq 1$, then $r^*_{WGS} \neq 0$ and $(\alpha_{r1,CO_2} r^*_{R1}) \neq 0$. Consequently MSRCO must be discarded as R1 since αSMRCO and CO_2 is zero.

The expression of the reaction rate for a reversible reaction can be written as

$$r_i = \frac{k_i \prod_j y_j^{\nu_{ij}} (1-\beta_i^{m_i})}{DEN}$$

$$\text{where } \beta_i = \frac{\prod_j y_j^{\alpha_{ij}}}{K_i^{eq}} y \quad DEN = 1 + \sum_h (K_h \prod_j y_j^{\mu_{hj}}), \quad m_i \geq 0 \tag{A.3}$$

Replacing Eq. (A.3) in (A.2)

$$\alpha_{R1,CO_2}(1-\beta^{m_{R1}}_{R1,*}) = \underbrace{-\left[\frac{k^*_{WGS}}{k^*_{R1}} \frac{\prod_j y_{j,*}^{\nu_{WGS,j}-\nu_{R1,j}}}{DEN_*}\right]}_{<0} (1-\beta^{m_{WGS}}_{WGS,*}) \tag{A.4}$$

The value of m has to be positive, $(1-\beta^m_{WGS}*) < 0$ (see Table A.1). Then from Eq. A.4, $\alpha_{R1,CO_2}(1-\beta^m_{R1}*) > 0$. As $(1-\beta^m_{R1}*) > 0$ for both MSR_{CO2} and MDR (see Table A.1), α_{R1,CO_2} has to be > 0. This condition only is satisfied by MSR_{CO2}.

Appendix B

Meaning of the kinetics coefficients and the equilibrium constants of the system

$$k_{E1} = k_7 C_T^0 2 K_1 K_2 K_3 K_4 K_8 K_{14} K_{16}^{1/2} K_{18}^{1/2}$$
$$\Rightarrow E_{E1} = E_7 + \Delta H_1 + \Delta H_2 + \Delta H_3 + \Delta H_4 + \Delta H_8 + \Delta H_{14} + \frac{1}{2}\Delta H_{16} + \frac{1}{2}\Delta H_{18}$$

$$k_{E2} = k_9 C_T^0 2 K_1 K_2 K_3 K_4 K_8 K_{12} K_{13} K_{14} K_{16} K_{18}$$
$$\Rightarrow E_{E2} = E_9 + \Delta H_1 + \Delta H_2 + \Delta H_3 + \Delta H_4 + \Delta H_8 + \Delta H_{12} + \Delta H_{13} + \Delta H_{14} + \Delta H_{16} + \Delta H_{18}$$

$$k_{R1} = k_{10} C_T^0 3 K_5 K_6 K_{12}^2 K_{13}^2 K_{16}^{2,5} K_{18}^{2,5} / (K_8 K_{14})$$
$$\Rightarrow E_{R1} = E_{10} + \Delta H_5 + \Delta H_6 + 2\Delta H_{12} + 2\Delta H_{13} + \frac{5}{2}\Delta H_{16} + \frac{5}{2}\Delta H_{18} - \Delta H_8 - \Delta H_{14}$$

$$k_{R2} = k_{11} C_T^0 2 / (K_{16}^{1/2} K_{17} K_{18}^{1/2}) \Rightarrow E_{R2} = E_{11} - \left(\frac{1}{2}\Delta H_{16} + \Delta H_{17} + \frac{1}{2}\Delta H_{18}\right)$$

$K_E = K_1$	$\Rightarrow \Delta H_E = \Delta H_1$
$K_{ETX} = K_1 K_2 K_{16}{}^{1/2} K_{18}{}^{1/2}$	$\Rightarrow \Delta H_{ETX} = \Delta H_1 + \Delta H_2 + \frac{1}{2}\Delta H_{16} + \frac{1}{2}\Delta H_{18}$
$K_{AC} = K_1 K_2 K_3 K_{16} K_{18}$	$\Rightarrow \Delta H_{AC} = \Delta H_1 + \Delta H_2 + \Delta H_3 + \Delta H_{16} + \Delta H_{18}$
$K_{CHO} = K_1 K_2 K_3 K_4 K_8 K_{14} K_{16}{}^{1/2} K_{18}{}^{1/2}$	$\Rightarrow \Delta H_{CHO} = \Delta H_1 + \Delta H_2 + \Delta H_3 + \Delta H_4 + \Delta H_8 + \Delta H_{14} + \frac{1}{2}\Delta H_{16} + \frac{1}{2}\Delta H_{18}$
$K_{CH_2} = K_5 K_{16} K_{18} / (K_8 K_{14})$	$\Rightarrow \Delta H_{CH_2} = \Delta H_5 + \Delta H_{16} + \Delta H_{18} - (\Delta H_8 + \Delta H_{14})$
$K_{CH} = K_5 K_6 K_{16}{}^{3/2} K_{18}{}^{3/2} / (K_8 K_{14})$	$\Rightarrow \Delta H_{CH} = \Delta H_5 + \Delta H_6 + \frac{3}{2}\Delta H_{16} + \frac{3}{2}\Delta H_{18} - (\Delta H_8 + \Delta H_{14})$
$K_{CH_3} = K_{16}^{1/2} K_{18}^{1/2} / (K_8 K_{14})$	$\Rightarrow \Delta H_{CH_3} = \frac{1}{2}\Delta H_{16} + \frac{1}{2}\Delta H_{18} - (\Delta H_8 + \Delta H_{14})$
$K_{H_2O} = K_{12}$	$\Rightarrow \Delta H_{H_2O} = \Delta H_{12}$
$K_{OH} = K_{12} K_{13} K_{16}{}^{1/2} K_{18}{}^{1/2}$	$\Rightarrow \Delta H_{OH} = \Delta H_{12} + \Delta H_{13} + \frac{1}{2}\Delta H_{16} + \frac{1}{2}\Delta H_{18}$
$K_{CH_4} = 1/K_{14}$	$\Rightarrow \Delta H_{CH_4} = -\Delta H_{14}$
$K_{CO} = 1/K_{15}$	$\Rightarrow \Delta H_{CO} = -\Delta H_{15}$
$K_H = 1/(K_{16}{}^{1/2} K_{18}{}^{1/2})$	$\Rightarrow \Delta H_H = -\left(\frac{1}{2}\Delta H_{16} + \frac{1}{2}\Delta H_{18}\right)$
$K_{CO_2} = 1/K_{17}$	$\Rightarrow \Delta H_{CO_2} = -\Delta H_{17}$
$K_{H_2} = 1/K_{18}$	$\Rightarrow \Delta H_{H_2} = -\Delta H_{18}$

$$K^{eq}_{R1} = \frac{k_{10} K_5 K_6 K_{12}^2 K_{13}^2 K_{16}^3 K_{17} K_{18}^4}{k_{-10}}$$

$$K^{eq}_{R2} = \frac{k_{11} K_{15}}{k_{-11} K_{12} K_{13} K_{16} K_{17} K_{18}}$$

then

$$\Delta H_{R1} = E_{10} + \Delta H_5 + \Delta H_6 + 2\Delta H_{12} + 2\Delta H_{13} + 3\Delta H_{16} + \Delta H_{17} + 4\Delta H_{18} - E_{-10}$$

$$\Delta H_{R2} = E_{11} + \Delta H_{12} + \Delta H_{13} + \Delta H_{15} + \Delta H_{16} + \Delta H_{17} + \Delta H_{18} - E_{-11}$$

The enthalpies of the equilibrium reactions were obtained from bibliography and correspond to their average value in the range of 873–923 K

$$\Delta \overline{H}_{R1} = 194.39 \frac{\text{kJ}}{\text{mol}}$$

$$\Delta \overline{H}_{R2} = -33.96 \frac{\text{kJ}}{\text{mol}}$$

Appendix C

Methodology employed to solve the system of differential equations

Due to the complexity of the system to be solved the estimation was conducted in the following three stages:

1. $\hat{y}^{Exp}_{j,z}$ variables were calculated from $y^{Exp}_{j,z}$ so as to satisfy the balance of C, O and H. The correction imposed on the

experimental mole fraction is the minimum according to the following correction function:

$$\phi = \sum_{z=1}^{N}\sum_{j=1}^{S}\left(\frac{\hat{y}_{j,z}^{Exp} - y_{j,z}^{Exp}}{y_{j,z}^{Exp}}\right)^2$$

with the restrictions applied to dilute systems

$$0 \le \hat{y}_{j,z}^{Exp} \le 1 \quad \forall j,z$$

$$(C.B): \sum_{j=1}^{S} \pi_{C,j} y_j^{inlet} - \sum_{j=1}^{S} \pi_{C,j} \hat{y}_j^{Exp} = 0$$

$$(O.B): \sum_{j=1}^{S} \pi_{O,j} y_j^{inlet} - \sum_{j=1}^{S} \pi_{O,j} \hat{y}_j^{Exp} = 0$$

$$(H.B): \sum_{j=1}^{S} \pi_{H,j} y_j^{inlet} - \sum_{j=1}^{S} \pi_{H,j} \hat{y}_j^{Exp} = 0$$

The parameters estimate was performed for each temperature and using the corrected values. This procedure simplifies the system and a smaller number of parameters – the middle – is estimated. In addition it can work with a smaller amount of experimental data at each temperature.The following verifications must be performed (Vanicce, 2005; Vanicce, 1979; Wojciechowski and Rice, 2003):

(a) the activation energies of the elementary stages must be positive
(b) $\Delta H_{ads}^0 < 0$
(c) $\Delta S_{ads}^0 = S_{ads}^0 - S_g^0 < 0$
(d) $|\Delta S_{ads}^0| < S_g^0$

2. The estimate is made at each temperature with the experimentally data, uncorrected for atomic balance, taking as a seed value to those obtained in the first step.
3. Finally all parameters at all temperatures were estimated using the experimental values, uncorrected for Lagrange, and taking as the seed value those obtained in the second step. Again it is verified that the adsorption enthalpies are negative and the activation energies of the elementary stages are positive. This values reported as the final estimate.

Nomenclature

C_T	total active sites concentration
D	reactor diameter
D_p	particle diameter
E_a	activation energy [kJ/mol]
F_j	molar flow of the j species [mol/min]
$F_{V,\ dry}$	total dry gas flow [ml/min]
$F_{V,T}$	total gas flow [ml/min]
F_T	total molar flow [mol/min]
H	enthalpy [kJ/mol]
k_i	kinetic coefficient of i reaction
K_j	adsorption constant of j species
K_i^{eq}	equilibrium constant of i reaction
L	reactor length
m_i	exponent in Eq. (A.3)
P	pressure [atma]
R	gas constant
R_j	yield of the j species
r_i	reaction rate of i reaction [mol/min mg]
r_j	reaction rate of j species [mol/min mg]
S_j	selectivity of the j species
S	entropy [kJ/mol K]
T	temperature [K]
W	catalyst mass [mg]
y_{et}	ethanol molar fraction
y_{H_2O}	water molar fraction
y_j	molar fraction of the j species

Greek letters

α_j	coefficient defined in Eqs. (3) and (4) ($\alpha CH_4 = \alpha CO = \alpha CO_2 = 2$; $\alpha H_2 = 6$).
α_{ij}	stoichiometric coefficient of the j species in the i reaction
β_i	defined in Eq. A.3
χ	ethanol conversion
χ_{H_2O}	water conversion
ΔH_i	reaction enthalpy of i reaction [kJ/mol]
ΔH_j	adsorption enthalpy of j species [kJ/mol]
ΔS_i	adsorption entropy [kJ/mol K]
μ_{hj}	exponent in Eq. A.3
ν_{ij}	reaction order of the j species in the i reaction
$\Pi_{C,J}$	number of C atoms in the j species
$\Pi_{H,J}$	number of H atoms in the j species
$\Pi_{O,J}$	number of O atoms in the j species
θ_V	space time [min mg/ml]
θ	space time [min mg/mol]

Subscripts and superscripts

ads	adsorbed
exp	experimental value
g	gas
i	reaction
in	inlet
j	species
out	outlet
sim	simulated value
z	experiment
0	standard
ˆ	corrected value

Acknowledgments

The authors wish to acknowledge the financial support received from Universidad de Buenos Aires, ANPCYT and CONICET.

References

Akande, A., Aboudheir, A., Idem, R., Delai, A., 2006. Kinetic modeling of hydrogen production by the catalytic reforming of crude ethanol over a co-precipitated Ni–Al_2O_3 catalyst in a packed bed tubular reactor. Int. J. Hydrogen Energy 31, 1707–1715.

Akpan, E., Akande, A., Aboudhier, A., Ibrahim, H., Idem, R., 2007. Experimental, kinetic and 2-D reactor modeling for simulation of the production of hydrogen by the catalytic reforming of concentrated crude ethanol (CRCCE) over a Ni-based commercial catalyst in a packed-bed tubular reactor. Chem. Eng. Sci. 62, 3112–3126.

Aupretre, F., Descome, C., Duprez, D., 2002. Bio-ethanol catalytic steam reforming over supported metal catalysts. Catal. Commun. 3, 263–267.

Aupretre, F., Descorme, C., Duprez, D., Casanave, D., Uzio, D., 2005. Ethanol steam reforming over $Mg_xNi_{1-x}Al_2O_3$ spinel oxide-supported Rh catalysts. J. Catal. 233, 464–477.

Batista, M.S., Santos, R.K.S., Assaf, E.M., Assaf, J.M., Ticianelli, E.A., 2004. High efficiency steam reforming of ethanol by cobalt-based catalysts. J. Power Sources 134, 27–32.

Bousiffi, M.A., Gunn, D.J., 2007. A dynamic study of steam-methane reforming. Int. J. Heat Mass Transfer 50, 723–733.

Busca, G., Montanari, T., Resini, C., Ramis, G., Costantino, U., 2009. Hydrogen from alcohols: IR and flow reactor studies. Catal. Today 143, 2–8.

Comas, J., Mariño, F., Laborde, M., Amadeo, N., 2004. Bio-ethanol steam reforming on Ni/Al_2O_3 catalyst. Chem. Eng. J. 98, 61–68.

Diagne, C., Idriss, H., Kiennemann, A., 2002. Hydrogen production by ethanol reforming over $Rh/CeO_2–ZrO_2$ catalysts. Catal. Commun. 3, 565–571.
Dömök, M., Tóth, M., Raskó, J., Erdohelyi, A., 2007. Adsorption and reactions of ethanol and ethanol-water mixture on alumina-supported Pt catalysts. Appl. Catal. B: Environ. 69, 262–272.
Fatsikostas, A., Verykios, X., 2004. Reaction network of steam reforming of ethanol over Ni-based catalysts. J. Catal. 225, 439–452.
Froment, G.F., Bishoff, K.B., 1990. Chemical Reactor Analysis and Design. Wiley, NY.
Graschinsky, C., Laborde, M., Amadeo, N., Le Valant, A., Bion, N., Epron, F., Duprez, D., 2010. Ethanol steam reforming over $Rh(1\%)MgAl_2O_4/Al_2O_3$: a kinetic study. Ind. Eng. Chem. Res. 49, 12383–12389.
Holladay, J.D., Hu, J., King, D.L., Wang, Y., 2009. An overview of hydrogen production technologies. Catal. Today 139, 244–260.
Hou, K., Hughes, R., 2001. The kinetics of methane steam reforming over a $Ni/\alpha\text{-}Al_2O_3$ catalyst. Chem. Eng. J. 82, 311–328.
Klouz, V., Fierro, V., Denton, P., Katz, H., Lisse, J.P., Bouvot-Mauduit, S., Mirodatos, C., 2002. Ethanol reforming for hydrogen production in a hybrid electric vehicle: process optimization. J. Power Sources 105, 26–34.
Mariño, F., Boveri, M., Baronetti, G., Laborde, M., 2004. Hydrogen production via catalytic gasification of ethanol. A mechanism proposal over copper–nickel catalysts. Int. J. Hydrogen Energy 29, 67–71.
Martin, D., Duprez, D., 1997. Evaluation of the acid-base surface properties of several oxides and supported metal catalysts by means of model reactions. J. Mol. Catal. A: Chem. 118, 113–128.
Mas, V., Dieuzeide, M.L., Jobbágy, M., Baronetti, G., Amadeo, N., Laborde, M., 2008a. Ni(II)–Al(III) layered double hydroxide as catalyst precursor for ethanol steam reforming: activation treatments and kinetic studies. Catal. Today 133–135, 319–323.
Mas, V., Baronetti, G., Amadeo, N., Laborde, M., 2008b. Ethanol steam reforming using Ni(II)–Al(III) layered double hydroxide as catalyst precursor. Kinetic study. Chem. Eng. J. 138, 602–607.
Mas, V., Bergamini, M.L., Baronetti, G., Amadeo, N., Laborde, M., 2008c. A kinetic study on ethanol steam reforming using a nickel based catalyst. Top. Catal. 51, 39–48.
Morgensen, D.A., Fornango, J.P., 2005. Low-temperature reforming of ethanol over copper-plated raney nickel: a new route to sustainable hydrogen for transportation. Energy Fuels 19, 1708–1716.
Phatak, A.A., Koryabkina, N., Rai, S., Ratts, J.L., Ruettinger, W., Farrauto, R.J., Blau, G.E., Delgass, W.N., Ribeiro, F.H., 2007. Kinetics of the water-gas shift reaction on Pt catalysts supported on alumina and ceria. Catal. Today 123, 224–234.
Profeti, L.P.R., Ticianelli, E.A., Assaf, E.M., 2009. Production of hydrogen via steam reforming of biofuels on $Ni/CeO_2–Al_2O_3$ catalysts promoted by noble metals. Int. J. Hydrogen Energy 34, 5049–5060.
Raskó, J., Hancz, A., Erdohelyi, A., 2004. Surface species and gas phase products in steam reforming of ethanol on TiO_2 and Rh/TiO_2. Appl. Catal. A: Gen. 269, 13–25.
Resini, C., Montanari, T., Barattini, L., Ramis, G., Busca, G., Presto, S., Riani, P., Marazza, R., Sisani, M., Marmottini, F., Costantino, U., 2009. Hydrogen production by ethanol steam reforming over Ni catalysts derived from hydrotalcite-like precursors: catalyst characterization, catalytic activity and reaction path. Appl. Catal. A: Gen. 355, 83–93.
Sahoo, D.R., Vajpai, S., Patel, S., Pant, K.K., 2007. Kinetic modeling of steam reforming of ethanol for the production of hydrogen over Co/Al_2O_3 catalyst. Chem. Eng. J. 125 (2007), 139–147.
Sun, J., Qiu, X.-P., Wu, F., Zhu, W.-T., 2005. H_2 from steam reforming of ethanol at low temperature over Ni/Y_2O_3, Ni/La_2O_3 and Ni/Al_2O_3 catalysts for fuel-cell application. Int. J. Hydrogen Energy 30, 437–445.
Vaidya, P.D., Rodrigues, A., 2006. Kinetics of steam reforming of ethanol over a Ru/Al_2O_3 catalyst. Ind. Eng. Chem. Res. 45, 6614–6618.
Vanicce, A., 2005. Kinetics of Catalytic Reactions. Springer Science Business Media Inc.
Vannice, M.A., Hyun, S.H., Kalpakci, B., Liauh, W.C., 1979. Entropies of adsorption in heterogeneous catalytic reactions. J. Catal. 56, 358–362.
Vizcaino, A.J., Arena, P., Baronetti, G., Carrero, A., Calles, J.A., Laborde, M.A., Amadeo, N., 2008. Steam reforming on Ni/Al_2O_3 catalysts: effect of Mg addition. Int. J. Hydrogen Energy 33, 3489–3492.
Wang, J., Lee, C., Lin, M., 2009. Mechanism of ethanol reforming: theoretical foundations. J. Phys. Chem. C 113, 6681–6688.
Wojciechowski, B.W., Rice, N.M., 2003. Experimental Methods in Kinetic Studies. Elsevier.
Xu, J., Froment, G.F., 1989. Methane steam reforming, methanation and water gas shift: I. Intrinsic kinetics. AIChE J. 35, 88–103.